UNCLASSIFIED

AD 408 702

DEFENSE DOCUMENTATION CENTER

FOR

SCIENTIFIC AND TECHNICAL INFORMATION

CAMERON STATION, ALEXANDRIA, VIRGINIA

UNCLASSIFIED

NOTICE: When government or other drawings, specifications or other data are used for any purpose other than in connection with a definitely related government procurement operation, the U. S. Government thereby incurs no responsibility, nor any obligation whatsoever; and the fact that the Government may have formulated, furnished, or in any way supplied the said drawings, specifications, or other data is not to be regarded by implication or otherwise as in any manner licensing the holder or any other person or corporation, or conveying any rights or permission to manufacture, use or sell any patented invention that may in any way be related thereto.

63-4-2

RADC-TDR-63-139

CATALOGED BY DDC
AS AD No. 408702

408 702

A FAST BROADBAND HIGH-POWER MICROWAVE SWITCH

by

Harry Goldie

Research Report No. PIBMRI-1111-63
Contract No. AF30(602)-2135
for
Rome Air Development Center
Research and Technology Division
Air Force Systems Command
United States Air Force
Griffiss Air Force Base
Rome, New York

February, 1963

JUL 8 1963
TISIA A

POLYTECHNIC INSTITUTE OF BROOKLYN
MICROWAVE RESEARCH INSTITUTE

ELECTROPHYSICS DEPARTMENT

PATENT NOTICE: When Government drawings, specifications, or other data are used for any purpose other than in connection with a definitely related Government procurement operation, the United States Government thereby incurs no responsibility nor any obligation whatsoever and the fact that the Government may have formulated, furnished, or in any way supplied the said drawings, specifications or other data is not to be regarded by implication or otherwise as in any manner licensing the holder or any other person or corporation, or conveying any rights or permission to manufacture, use, or sell any patented invention that may in any way be related thereto.

Qualified requestors may obtain copies of this report from the ASTIA Document Service Center. ASTIA Services for the Department of Defense contractors are available through the "Field of Interest Register" on a "need-to-know" certified by the cognizant military agency of their project or contract.

RADC-TDR-63-139

Report No. PIBMRI-1111-63
Contract No. AF30(602)-2135

A FAST BROADBAND HIGH-POWER MICROWAVE SWITCH

by

Harry Goldie

Polytechnic Institute of Brooklyn
Microwave Research Institute
55 Johnson Street
Brooklyn 1, New York

Research Report No. PIBMRI-1111-63
Contract No. AF30(602)-2135

11 February 1963

Title Page
Acknowledgement
Abstract
Table of Contents
List of Figures
18 Pages of Text
Appendices
Bibliography

Harry Goldie
Research Assistant, Sr.

Approved:

John W. E. Griemsmann
Professor

Prepared for
Rome Air Development Center
Research and Technology Division
Air Force Systems Command
United States Air Force
Griffiss Air Force Base
Rome, New York

FOREWORD

I wish to thank Mr. A. E. Gordon, chief engineer at Kuthe Laboratories for his continued support and assistance in fabricating the anode and cathode assemblies and for their cooperation in experimentally determining the size of grid apertures. Thanks is also due Mr. B. Ford for his computational work and the plotting of the curves in the report.

The work contained in this report was sponsored by the Rome Air Development Center, Air Force Systems Command, Griffis Air Force Base, Rome, New York under Contract No. AF-30(602)-2135.

The work took place at the Microwave Research Institute of Brooklyn, New York; The Long Island Graduate Center, Farmingdale, New York and the Kuthe Laboratories, Inc. of 730 South 13th Street, Newark, New Jersey over the period from December, 1960 to October, 1962.

ABSTRACT

This report describes the design and development of a broadband, high power, low-pressure microwave switch. Pertinent design information, particularly as it relates to electrical performance and mechanical fabrication is presented, as is detailed information on the experimental measurement facilities.

Particularly significant results derived are the magnitude of the peak pulse microwave power that the gaseous switch can control and the rapidity of switching action. Other features are the low insertion loss with the device either in the active or passive state. Good isolation was achieved over the entire range of rated power level. The following experimental results were achieved:

1.	Rf power switched	up to a megawatt
2.	Switching Time	30 nanoseconds
3.	Isolation	30 decibels
4.	Arc Loss	0.9 decibels
5.	Cold Insertion Loss	0.2 decibels
6.	Spike Leakage	none
7.	VSWR (over C band)	1.2 (max)
8.	Recovery Time	30 microseconds
9.	RF Pulse Width	up to 1 microsecond*

*May be extended to larger durations but switching peak power decreases. For example, at 3.25 microsecond width the switching capacity is 1/3 of a megawatt.

TABLE OF CONTENTS

LIST OF FIGURES

I. Introduction

This report describes the results of an investigation into the feasibility of developing a fast, broadband voltage-controlled, microwave gas switch capable of switching pulsed microwave power. There are several ways to switch microwaves, such as ferrite faraday rotators, devices that utilize the B-H loop of ferrites, high-vacuum cavities employing the multipactor effect or low-pressure gaseous devices. In this study the gaseous method was employed. At the time of this choice, available data suggested that gas switching offered low cold insertion loss and relatively fast switching over a broad band of frequencies in the microwave range. There was little evidence available to predict the pulse power handling capability of the gaseous switch in the low pressure range. Some work had been done on a similar device[1], but this design was used only to switch relatively low-power levels.

Also at this time the temperature dependence of ferrites limited their high power capabilities, and the isolation of ferrite switches was considerably less than that of gaseous devices. Mechanical switching was rejected because of the very slow switching times, of the order of milliseconds.

Gaseous devices now used in duplexers are not dc voltage-controlled but depend on the microwave power level for operation. Other gas devices utilizing the glow discharge to control either phase shift[2] or attenuation[3] have power limitation in that control is lost for high incident powers. In the approach used here a gas-filled triode tube was designed where the control grid served the dual purpose of guiding the electromagnetic waves and receiving the d.c. trigger voltage to initiate the grid-cathode plasma. The switch tube is depicted in figure 1. This tube was proposed, designed, constructed and tested. The testing yielded the following data for the TWS:†

1.	RF Power Switched	1 megawatt
2.	Switching Time*	30 nanoseconds
3.	Isolation	30 decibels
4.	Arc-loss	0.9 decibels
5.	Cold Insertion Loss	0.2 decibels
6.	Spike Leakage	none
7.	VSWR (over C-band)	1.2
8.	Recovery Time	30 microseconds
9.	RF Pulse Width	1.0 microsecond

*Definitions are given in section 2.
†TWS refers to Triggered Waveguide Switch

II. Definitions and Symbols

In general, microwave energy entering any component at a Point A and leaving at a point B experiences a loss between points A and B. The distribution of power is shown below:

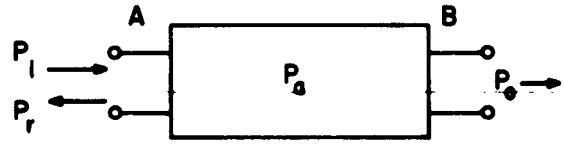

Distribution of Power in a Two-Terminal Network

The terms involved are:

P_i = the power incident at terminal A

P_o = the output power at terminal B

P_r = the total power reflected from the component when the output line is terminated in its characteristic impedance.

P_a = the total power absorbed in the component.

These definitions apply to a two-terminal pair network. It should be observ that in the cases where higher order waveguide modes exist at a physical termination of the network, each mode should be considered separately. In this report only the TE_{10} mode, the dominant mode in rectangular waveguide, is considered. Thus conservation of energy requires that:

(2-1) $$P_i = P_r + P_o + P_a$$

The following definitions apply between terminals A and B:

With the block in the passive state -

(2-2) $$\text{Cold Insertion Loss} = 10 \log P_i/P_o$$

With the block in the active state -

(2-3) $$\text{Absorption Loss} = 10 \log P_i/P_r$$

when the transmitted power is negligible. The absorption loss includes all losses within the block, i.e., the rf power absorbed by the gas (this is arc-loss), waveguide wall losses, radiation, etc. The dominant loss here is the power absorbed in the active state, referred to as "arc-loss".

(2-4) $\text{Isolation} = 10 \log P_i/P_o$

The definition of the breakdown of a gas under the influence of an adequately high intensity electric field will be defined as the transition of the electron density in the gas from a relatively low initial value to a density (several orders of magnitude greater) at which the rate of production of electrons and the rate of loss of electrons are equal, thus establishing a steady state.

Symbols used in the report are:

α = ionization coefficient
ε = dielectric constant
μ_o = permeability of free space
Λ = characteristic diffusion length
λ_g = wavelength in free space
ω_p = plasma resonance frequency
ω = waveguide angular frequency
μ = mobility
ν_i = ionizing collision frequency
ν_c = elastic collision frequency
ν = total collision frequency
τ_{RF} = duration of waveguide field pulse
τ_D = de-ionization time
τ_p = duration of tube current pulse
σ = conductivity

p_o = pressure normalized to 0°C
p = pressure at any temperature
u_i = ionization potential
$\bar{u}$ = average electron energy
d = length of switch tube
x = electron displacement
t = time
m = mass of electron

e = electronic charge
N = electron density
E_o = r.f. electric field
J = current density
P = microwave power
b = dummy variable
D = diffusion coefficient
$\bar{v}_d$ = drift velocity of electrons
T_s* = r.f. dynamic switching time

III. Theoretical Discussion

3-1. Discussion of Plasma Resonance
3-2. Transmission Equations
3-3. Switch Tube

3-1. Discussion of Plasma Resonance

The properties of gaseous switching depend upon certain fundamental parameters. A discussion of the factors which significantly affect the ability of an established plasma to reflect microwaves is given.

Consider a rectangular waveguide closed off at both ends by windows in which a wave is propagating in the TE_{10} mode. The gas is assumed to be ionized and the electron density N is assumed to be uniform. If P_o' is the power entering the ionized gas, then

(3-1) $$P_o' = P_i - P_r$$

This can be written as

$$\frac{E_o' H_o'}{2} = \frac{E_i H_i}{2} - \frac{E_r H_r}{2}$$

since the peak transverse magnetic field and electric field are normal and in phase with each other. In terms of Z_o

(3-3) $$\frac{E_i^2}{2Z_o} - \frac{E_r^2}{2Z_o} = \frac{E_o'^2}{2Z_o'} \quad \text{and}$$

*It is defined as the time elapsed for the reflected pulse to increase from a relatively low level to a relatively high level; that is, from the 10% to 90% points on the detected envelope.

(3-4) $$E_i^2 - E_r^2 = E_o^2$$ then

(3-5) $$\left(\frac{E_o'}{E_o} \right)^2 = \frac{Z_o'}{Z_o}$$

where E_o' and Z_o' are the electric field and the wave impedance in the ionized gas-filled waveguide, and E_o and Z_o are the electric field and wave impedance of the empty waveguide. The wave impedance may be written in the form:

(3-6) $$Z_o = \frac{\lambda_g \omega \mu_o}{2\pi}$$

where λ_g is the waveguide wavelength. Substituting Z_o, we get

(3-7) $$\frac{E_o'^2}{E_o^2} = \frac{\lambda_g'}{\lambda_g}$$

where λ_g' is the guide wavelength in the ionized gas. Then the ratio of electric fields determines the wavelength in the gas. An increase in E_o'/E_o results in a waveguide-below-cutoff. The increase in E_o' comes about by achieving a condition of plasma resonance, of which a simplified and brief discussion follows:

An ideal method for rapidly switching microwave power would be an arrangement whereby a thick sheet of electrons would fill an evacuated waveguide in near-zero time. Free electrons in a vacuum oscillate 90° out-of-phase with the microwave electric field incident upon it, and ideally, no energy is absorbed from the field. The equation of motion of an electron acted upon by a microwave sinusoidally varying field $E_o \cos \omega t$ is:

(3-8) $$m \frac{d^2x}{dt^2} = e E_o \cos \omega t$$

Integrating this and dividing by m gives the current

(3-9) $$i = e \frac{dx}{dt} = \frac{e^2 E_o \sin \omega t}{m\omega}$$

The current density is

(3-10) $$J = \frac{Ne^2}{m\omega} E_o \sin \omega t$$

From the above, the electron current is out of phase with the electric field, and the conductivity is purely imaginary. The electron gas is characterized by a

dielectric constant

$$\varepsilon = \varepsilon_o \left(1 - \frac{\sigma_i}{j\omega\varepsilon_o} \right) \tag{3-11}$$

The conductivity is imaginary (σ_i) and is

$$\sigma_i = \frac{J}{E} = \frac{Ne^2}{j\omega m} \qquad \text{where } E = E_o \sin \omega t \tag{3-12}$$

Substitution of (3-12) into (3-11) leads to

$$\varepsilon = \varepsilon_o \left(1 - \frac{\omega_p^2}{\omega^2} \right) \tag{3-13}$$

where

$$\omega_p^2 = \frac{Ne^2}{m\varepsilon_o} \tag{3-14}$$

Note that when plasma resonance (ω_p) exceeds the signal frequency (ω), the dielectric constant of the electron gas becomes negative. It is this condition of a negative permitivity which causes the r.f. electric field, E_o', to increase. In accordance with the previous discussion, one has a waveguide-below-cutoff and reflection from the plasma occurs; i.e., switching action is achieved. A more rigorous derivation of the dielectric constant which includes the damping term due to collisions may be found in the latter part of Appendix I.

3-2. Transmission Equations

A qualitative view of the transmission characteristics of the switch tube can be formulated from transmission line impedance considerations. The significant approximations are given below; and the derivations are given in the Fourth Quarterly Report[4] and are repeated in Appendix I of this report.

a) The waveguide is assumed to contain an isotropic dielectric of uniform density.

b) The effects of geometry on wave modes is entirely neglected; i.e., a TEM mode is assumed instead of the actual TE_{10} mode.

The equations are given as follows:

$$T = 10 \log \frac{P_T}{P_I} = 10 \log \left[\frac{4b \exp j3\pi b/2}{(1+b)^2 - (1-b)^2 \exp j\, 3\pi b} \right]^2 \tag{3-15}$$

$$(3\text{-}16) \qquad R = 10 \log \frac{P_R}{P_I} = 10 \log \left[\frac{(1-b)^2 (1 - \exp j3\pi b)}{(1+b)^2 - (1-b)^2 \exp j3\pi b} \right]^2$$

$$(3\text{-}17) \qquad b = \left[1 - \frac{\omega_p^2}{\omega^2 + \nu_c^2} + j \frac{\nu_c}{\omega} \frac{\omega_p^2}{\omega^2 + \nu_c^2} \right]^{1/2} = \left[\frac{\varepsilon_c}{\varepsilon_o} \right]^{1/2}$$

$$(3\text{-}14) \qquad \omega_p^2 = \frac{Ne^2}{m \varepsilon_o}$$

The above equations have been plotted and are depicted as follows:

Equation	Depicted In Figure	Independent Variable	Dependent Variable	Parameter
4-15	3	ω_p/ω	T	ν_c/ω
4-16	4	ω_p/ω	R	ν_c/ω
4-17	2a	ω_p/ω	$\varepsilon_{imaginary}$	ν_c/ω
4-18	2b	ω_p/ω	ε_{REAL}	ν_c/ω

3-3. The Switch Tube

The essential requirement of the switch tube is to establish an electron density in the waveguide independently of the r.f. field. It must be of sufficient magnitude to reflect almost all of the incident microwave power and to absorb very little. The creation of this electron density must be accomplished in an interval of time much shorter than r.f. pulse widths normally employed in microwave systems.

The dc voltage-controlled switch tube depicted in figure 1 is essentially a gas-filled thyratron where the tube body serves the dual role of (a) guiding the electromagnetic waves and (b) serving as the control grid of the triode. The operation may be explained as follows:

1. The applied trigger pulse causes breakdown of the grid-cathode space leading to the growth of a plasma near the grid apertures.
2. Electrons from this plasma are accelerated in the anode space causing ionization. The ionization leads to a cumulative modification of the original potential distribution, resulting in anode breakdown and establishment of a conducting channel through the apertures.

Upon application of a grid trigger potential there is a delay of a few tenths of a microsecond, then grid current begins to increase. When the grid current reaches a certain critical value, conduction is transferred to the anode and the commutation interval starts. A plasma forms in the waveguide. The anode voltage then falls to a very low value with a time constant of a few hundredths of a microsecond. The tube current begins to rise at a rate determined by

(a) the modulator circuit time constant

(b) the rate of fall of anode voltage and magnitude of anode voltage

(c) the pressure

During the steady conduction interval the anode voltage is substantially constant and equal to the tube drop. At the end of this time the pulse forming network has delivered it's charge and the tube current falls to zero. The electron density is the combination of the electron gas in the plasma and the charge of the PFN. After the termination of the tube's current pulse, the electron density is only a function of the decay time of the plasma.

IV. Breakdown at High Frequency

The peak power handling capacity of the switch tube is determined by the maximum r.f. electric field that the tube can pass without initiating a microwave-induced discharge. An understanding of the controlling mechanisms of an r.f. discharge in a low pressure gas is of importance in determining methods which can be used to increase the power-handling capacity of the switch.

The breakdown criterion for pulsed gas discharge can be found by considering the factors that lead to the threshold of breakdown. Brown[7] has developed a breakdown criterion for a c.w. microwave discharge at low pressures and has experimentally verified his theoretical result. His result was derived from the diffusion equation

$$\frac{\partial N}{\partial t} = P_e - L_e \tag{4-1}$$

by setting $\partial N/\partial t = 0$; i.e., $P_e = L_e$. P_e is the electron production rate and L_e is electron loss rate.

The breakdown field predicted by Brown was a function of gas type, pressure, geometry and wavelength of the c.w. applied field.

The quantitative c.w. theory considered above is not valid when r.f. pulses are employed to induce breakdown. The condition that there exists a balance between ionization rate and loss rate does not hold since breakdown must occur within a definite time interval. The effect of initial density N_o, the applied field repetition rate,

and the step field duration becomes significant. The characteristic diffusion length, wavelength and average electron energy assume little significance. Initial density is not accounted for in the c.w. theory because the free electrons are allowed to build up in an infinite time. In practice, an infinite time is not allowed for the density buildup but a field slightly higher than the threshold field is used to produce breakdown.

The solution of the continuity equation accounting for pulse-type breakdown is*

$$\frac{1}{p\tau_{R.F.}} \ln \frac{N_b}{N_o} = \frac{\nu_i}{p} - \frac{Dp}{(p\Lambda)^2} \tag{4-2}$$

where N_b is the electron density at breakdown.

Under all conditions the pulsed breakdown field will be greater than the corresponding c.w. breakdown field. In the limit of low PRR and long pulse width the breakdown field approaches the c.w. breakdown field. As the pulse width is shortened, the field required for breakdown increases. This is due to the time it takes for the electrons to absorb energy from the stepfield (the rise time of the stepfield may be neglected). If the energy equilibrium time between the field and the free electrons is greater than the pulse duration, breakdown will not occur. To induce breakdown in a shorter time, the electrons may be overexcited by employing r.f. fields many times the threshold value. The large fields will supply the electron energy losses, the four most important losses being, in our low pressure range,

(a) diffusion to the walls
(b) elastic collisions
(c) ionizing collisions
(d) excitation

The latter discussion concerned the pulse width dependence on breakdown; the following discussion considers the applied pulse repetition rate and initial electron density.

Application of a series of r.f. pulses at a given PRR has the effect of lowering the breakdown field. In the limit of low PRR (for a given pulse width) the breakdown field is greatest. The field decreases with increasing repetition rate. This is due to electrons produced in one pulse affecting breakdown conditons for the succeeding pulse. When the decay of electrons in the afterglow is complete between pulses, the breakdown field will be insensitive to the PRR. The decay in the afterglow is controlled by ambipolar diffusion except at the very lowest values of electron density where a transition from ambipolar to free diffusion occurs.

*See Appendix for derivation.

V. Practical Considerations of the Grid-Controlled Switch Tube

5-1. Switch Tube Construction

5-2. Modulator Design

5-3. Microwave Test Facility

5-1. Switch Tube Construction

Mechanically, the switch tube is essentially a short section of standard rectangular copper waveguide, suitably perforated for grid operation, with the ends sealed off by microwave pressure windows. An anode and cathode is attached to the upper and lower broad walls concentric with the perforations to form the tube. These assemblies are enclosed by a vacuum-tight ceramic envelope. Figure 5 illustrates the tube in an exploded view. Figure 6 is a photograph of the switch tube.

The waveguide body was machined from OFHC waveguide. This oxygen-free material is essential for gaseous devices since heating the copper will cause oxygen molecules to be liberated from the surfaces and contaminate the hydrogen. The OFHC copper is also necessary for brazing operations in an inert or hydrogen atmosphere. The grid holes were drilled first, and then the kovar self-centering heliarc ring was brazed concentric to the grid. This was done using a nickel-gold-copper brazing flux at a temperature of 1060° C. The mating ring to this heliarc ring is then attached to the anode and cathode assembly in a separate operation. One of the complications in the fabrication of the switch tube was the attachment of the waveguide windows at each end of the waveguide. The waveguide windows were especially designed for this tube. They are made of kovar and 707 glass and are of triple-iris design for high mechanical strength. The bakeout temperature of the tube, dictated by the type of cathode, was 450° C. Thus the temperatures that these windows must safely withstand should be 700° C. The windows had to be attached at an intermediate temperature which was selected to be at 600° C. A type R.N. solder was used and the welding was done in a hydrogen atmosphere. Special jigging was required and this resulted in several failures before the successful tube was brazed. The waveguide body at this stage of construction could easily withstand the planned bakeout temperature of 450-500° C. The last remaining mechanical process was the attachment by a heliarc weld of the entire anode and cathode assemblies. These assemblies were completed and the heliarc ring was brazed to the ceramic envelope inside of a bell jar by an induction heating weld. The ring attached to the waveguide itself had a maximum outer diameter of 1.875 inches. Figure 1 illustrates the heliarc weld. The anode assembly is OFHC copper with a molybdenum plate for mechanical strength. This plate is bonded on to the anode cup as illustrated in Figure 1. The cathode assembly consists of the cathode, cathode-baffle, cathode heat shield, heater and the titanium hydride reservoir. The exhaust

tubulation can also be seen. The spacing of the anode-upper grid was 0.100 inch dictated by the maximum voltage that the pulse-forming network can handle and is a fundamental specification. The distance between the lower grid and cathode-baffle was approximately 0.900 inches and is not critical. Too close a spacing would require abnormally high grid potentials to initiate a plasma in the lower grid-cathode region. Too large a spacing would merely make the tube physically large. The thickness of the two control grids was chosen as small as possible within the bounds of mechanical strength. The selected value was 0.040 inches with each hole 0.125 inches in diameter.

The final assembly was baked out and exhausted. No leaks were detected. The unit was heated in a bell jar to 450° C and the long process of outgassing began. This procedure is essential for an uncontaminated active cathode. The effective cathode area was approximately 12-14 square centimeters. The tube was then pumped down to a pressure of 0.1 microns and the aging process was initiated. The tubulation was pinched off, and the tube was cleaned and plated. Following the aging test, potentials were applied and preliminary d.c. measurements were performed.

5-2. Modulator Design

The purpose of the modulator is to supply the necessary voltages and currents to operate the grid-controlled switch tube. A simplified diagram with a schematic is presented in Figure 7.

The principal elements requiring attention in the design are the:

(a) pulse-forming network
(b) the load resistor
(c) the grid signal system
(d) the charging system

a) The pulse forming network used was a section of 50 ohm cable cut to a length which gave a two-way delay time of one microsecond. Hence, the elapsed time between the formation of the conducting path through the tube and the termination of the complete discharge of the network is one microsecond.

b) The load resistor, aside from dissipating the pulse power satisfactorily, should be insensitive to frequency up to the highest components in the load pulse.

c) The trigger generator, synchronized from a timing oscillator, pulses the control-grid through a filter (de-spiking network) circuit. The trigger amplitude was readily adjustable. The instrumentation is diagramatically depicted in Figure 8. A one-ohm spoke resistor, designed for minimum inductance, was used to oscillograph the rise of cathode current.

d) The basic considerations involved in the design of the charging system is the method by which charge is added to the PFN, and the rate at which the PFN is charged. A charging diode is used to insure that the PFN current discharges through the tube and not through the charging system. The path of the discharge current is shown in Figure 7 by the arrow denoting i_p.

5-3. Microwave Test Facility

Figure 8 depicts the r.f. test facility to examine the operating characteristics of the switch. Basic considerations are the accurate measurement and determination of:

(a) peak power handling capacity
(b) r.f. dynamic switching time
(c) rate-of-rise of tube current
(d) isolation, cold and hot insertion losses
(e) de-ionization time

The average power was measured (off a calibrated directional coupler) and then converted to peak power by calculation. Highly stable, temperature-compensated thermistors were used. The overall accuracy of power measurement was probably no better than $\pm$ 10%.

The switching times were measured by observing the rise time of the reflected pulse when clipped or the fall time of the transmitted pulse. Refer to the second oscillogram of Figure 10.

The test setup was flexible in that the r.f. pulse could be advanced or delayed with respect to the tube trigger pulse. Thus with a triggered plasma (thyratron discharge) occuring in the waveguide the electromagnetic field could be adjusted to arrive as shown:

RF PULSE ARRIVAL TIME	SWITCHING POSSIBLE
(a) before the thyratron discharge occurs	No
(b) during the tube current pulse interval	Yes
(c) in the afterglow period following the cessation of tube current	Yes
(d) after the termination of the afterglow	No

VI. Experimental Data and Data Analysis

6-1. Experimental Data

The waveforms of the switch tube are depicted in Figure 9, where the rate-of-rise of tube current is given. Typical switching data is given in Figure 11. Figure 12 is a plot of the data of Figure 11. The switching time was found to be a sensitive function of the anode potential. This dependence is graphically illustrated in Figure 13. The r.f. dynamic switching time is defined on this curve. Figure 10 depicts switching oscillograms. Figure 14 shows the dependence of the threshold-of-breakdown value on the tube potentials. Figure 15 reports the de-ionization times.

6-2. Data Analysis

The magnitude of the electromagnetic stepfield that the tube could holdoff was observed to be 13 rms kv/cm (1.9 megawatts) and the duration of this field was 0.7 microseconds. Higher peak power levels than this caused a microwave initiated discharge in the waveguide. A relatively low gas-pressure was used. Very low pressures required enormous dc trigger potentials on the grid to initiate thryratron action. When thryratron action was initiated by a relatively high value of grid-cathode trigger potential ineffective switching occurred. Isolation was poor at this level, and during the switching interval intermittent arcing occurred which ultimately resulted in high absorption losses.

What may have been the reason for this arcing is as follows: since the operating pressure was very low, the mean free electron path (MFP) was probably greater than the grid-to-grid dimension. We note that when the grid-cathode trigger potential was not applied, no arcing occurred at the very high r.f. power levels. In this case, the negative bias on the grid kept high-velocity initiatory electrons out of the waveguide and an rf induced discharge could not begin. On the other hand, when the negative bias was overcome by a high-potential trigger applied to the grid, high-velocity initiatory electrons were introduced into the waveguide space through the lower grid apertures. Accelerated by the anode field through an MFP exceeding tube dimensions the electrons attain very high velocities. All conditions for field emission discharges are met at these long MFP and intense electric fields. It is probable that field emission was the mechanism which caused the breakdown. In fact, white filamentary sparks which appeared near the grid holes and extended from grid-to-grid were visually observed through the microwave glass pressure windows. Multipactor phenomena was ruled out as the primary mechanism because of the presence of the dc field; and Townsend discharges will not occur at these low pressures.

These effects were less pronounced at lower r.f. field levels. When the field was lowered, the pressure could be increased slightly without an r.f. discharge occurring. This allowed easy triggering of the grid for thryatron action. The field level

at this operating point was 10 rms kv/cm (1180 kilowatts). The external switching characteristics were good at this level; hence, the switch tube carries a nominal rating of one megawatt. The data is presented in Fig. 11.

In Figure 14 the threshold-of-breakdown is given for a pressure of approxi- 0.2 mm of Hg. The field value is 5.4 rms kv/cm (334 kilowatts). In this experiment the tube was subjected to an electromagnetic stepfield which traversed the gas-filled waveguide. The threshold-of-breakdown value occurred when the transmitted pulse's attenuation increased from a relatively low value (0.2-0.3 dbs) to a relatively high value (30 dbs). In addition, a visible glow is seen through a sighting tube; the instrumentation is depicted in Fig. 8. In this data the threshold field is a function of the grid bias, as shown at the lower part of the table, and anode potential as shown in the upper part of the table.

In order to explain why there is a slight increase in rf threshold-of-breakdown electric field (top half of table II), one must note that, previous to breakdown, the percentage of anode field lines terminating on the lower grid is a small fraction of that terminating on the upper grid. What we then have is, as far as the waveguide gas volume is concerned, a dc sweeping field. This sweeping field decreases the number of initiatory electrons before the r.f. intense stepfield arrives. Reference to equation (A2-3) in Appendix II denotes the threshold field goes as $\ln N_B/N_o$; a very slowly varying quantity even with decade changes of N_o, the initiatory electron density. This probably explains the reason for a small increase in threshold fields with the large changes in sweeping field.

The same agrument used above can be utilized to explain the large increase in the rf threshold-of-breakdown (see bottom of table II) with increasing negative grid bias with constant anode field. The significant difference here is the bias voltage controls both the number and velocity of initiatory electrons into the waveguide space from the hot cathode. When the bias voltage is relatively large and the anode voltage is held constant at some high value, the rf holdoff field is a maximum. This is due to the combination of anode sweeping field and the grid potential barrier developed. The large value of bias prevents electrons from entering the waveguide region so that the only source of initiatory electrons is that due to cosmic rays, inter-atomic collisions (Saha collisions), etc.

When the bias is reduced somewhat, the breakdown field is reduced in qualitative accordance with $\ln N_B/N_o$. When it is reduced to zero, many of the energetic electrons from the cathode enter the waveguide space by virtue of their thermal volocities (and perhaps influenced by a small fraction of anode field which penetrates the cathode region). This causes the breakdown field to decrease by as much as 40%. If the anode field is reduced to zero for the condition of zero grid bias, the breakdown

field further reduces. This last point is not verified on the data sheet but may be deduced from the complete data on table II in conjunction with the qualitative discussion above.

As a final statement; if a method can be devised which can prevent all initiatory electrons from appearing in the waveguide space prior to and during rf wave incidence, the holdoff field approaches infinity.

The cold insertion loss is a function of the VSWR, wall losses, radiation and rf power absorption of the gas. The value was small, as expected, since the switch in the unionized state is transparent to microwaves and acts as a low loss section of waveguide. See Fig. 12.

The hot insertion loss (combination of the cold insertion loss plus the r.f. energy required to maintain and intensify the discharge) was moderate and did not exhibit sharp fluctuation over the incident peak power range of the switch. The greatest part of this switch loss is the r.f. absorption, probably accounting for about 0.7 db of the total 0.9 db. See Fig. 12.

The isolation, a number indicating the amount of power being transmitted past the switch when a plasma is formed, was about 30 dbs, or only 0.1% of the incident power. The isolation can be directly interpreted to give the average value of electron density during the switching interval. The (experimental) ratio of $\nu_c/\omega = .033$ when the pressure is 0.2 mm of Hg. From L. Goldstein's[5, 8] work, the plasma density may be found and is 8×10^{11} electrons/cc.

The recovery time, a factor primarily dependent on tube geometry (see Fig. 15 and eq. 4-7), was obtained experimentally by employing a low-power probing generator at a c.w. frequency of about 5gcs. The measured recovery time was 30 microseconds and varied little with changes of anode voltage (1 - 3kv) and pressure (approximately 0.1 - 0.3 mm of Hg).

The recovery time is seen to increase slowly with increasing anode voltage. One reason for this is the higher electron densities achieved by increasing the dc peak current through the tube. The recovery time also shows some dependence on pressure. This is to be expected since increasing the gas pressure increases the gas density and hence, also the dc peak current through the tube (assuming tube potentials are held constant). The deionization time, in turn, is a function of the initial electron density which decays exponentially from the initial value N_o^* according to the relation $N = N_o \varepsilon^{-t/\tau}$, where $\tau = \Lambda^2/D_a$, is the decay time constant, Λ the diffusion length and D_a the ambipolar diffusion coefficient. The time required to reach a particular value of N is the decay time and is proportional to log (N/N_o). It is seen to depend both on the initial electron density N_o and on τ.

*This initial value is the maximum value of N_o achieved in the discharge and is not to be confused with the initiatory electrons discussed on pages 13 and 14.

The insensitivity of recovery time to applied negative grid bias for small ranges of grid bias voltage is shown in the lower part of table III. The negative bias on the grids causes a positive ion sheath to appear in the grid apertures. This prevents electrons from entering the waveguide region removing the possibility of further ionization. Qualitatively this means that the deionization time is essentially a function of the geometry (which determines Λ), the diffusion coefficient (D_a) and the value of electron density N_o at the cessation of the tube current pulse.

The actuating time of the switch was found to be a sensitive function of the static anode potential and an insensitive function of pressure except at extremes. The curve of r.f. dynamic switching time as a function of anode potential is given in Figure 13. The reason for this sensivity is the influence of the anode field lines on the electrons ejected into the waveguide space by the positive grid trigger pulse. The electrons attain high kinetic energies rapidly traversing the waveguide toward the anode where a plasma begins to form. This plasma, highly conductive, "extends" the anode toward the cathode resulting in a plasma filling the waveguide in a very short time. The nominal switching time is approximately 30 nanoseconds.

Noise Temperature

Since the TWS (thyratron triggered waveguide switch) in certain applications may be part of a low noise microwave receiving system, an attempt to rate the noise temperature from existing data will be made. The noise temperature will be considered uniform over the waveguide space of the TWS. Basically we ask, "What is the noise power output change of the TWS when inserted between a source and an output port in the "on" "off" states?". If the power absorbing component appears as follows:

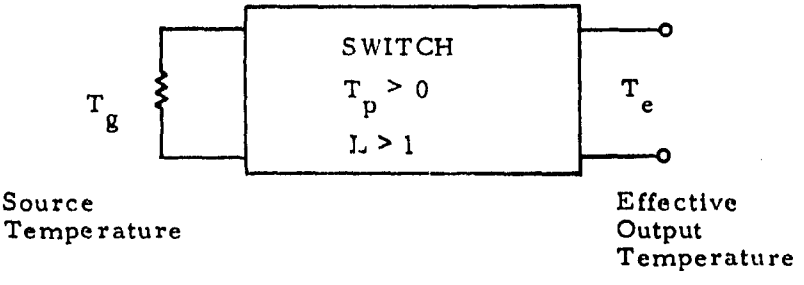

then the effective temperature T_e is given as:[1]

$$T_e = T_p (1 - 1/L) + T_g/L$$

where T_p is the operating temperature of the TWS in ^oK.

Using the above relation which states that the effective temperature T_e is proportional to the noise output of the source plus the component under test, the following table may be computed based on measured data:

Switch	Measured Loss		*T_g	T_p	T_e
Mode	dbs	L	^oK	^oK	^oK
On	0.70	1.175	0	325	48.5
Off	0.10	1.047	0	325	14.3

*By assuming that $T_g = 0\ ^oK$ the noise temperature contribution of the TWS is found.

Noise contributions due to thermonic emission of the grid are expected to be low because of the large grid radiating area resulting in cool operation. The cathode is completely baffled and one would expect very small noise contributions from cathode material sputtering on other electrodes within the TWS.

Life

The significant factors affecting the TWS lifetime are:

a) window deterioration

b) gas cleanup

c) internal electrode sputtering

Upon close examination of the tube, it was noted that a thin deposit of material accumulated on the vacuum side of the windows; a check on the low power VSWR and insertion loss characteristics revealed no substantial changes. High power operation remained unaffected. This deposit has formed while operating after a period of approximately 125 hours. The windows continue to perform their intended job satisfactorily.

Gas cleanup is non-existent because of the use of an adjustable titanium hydride reservoir which maintains a constant pressure. This reservoir has been used in many types of commercial thyratrons. Use of low-vapor-pressure materials and a rigorous outgassing-bakeout procedure has minimized the possibility of gas impurities.

Sputtering, which can shorten the life of anodes and cathodes, is minimized here because of the complete baffling of the cathode from the remaining electrodes. An active cathode is essential to switch tube operation. Anode deterioration is minimized because of the use of a molybdenum plate which is highly resistant to distruction by sputtering. This plate is bonded to the OHFC copper electrode which comprises the anode assembly.

The TWS was built and first tested in July of 1962. During the past ten months it has operated satisfactorily for 150 hours, though not for more than 6 hours on a continuous basis. The tube appears to have lifetime comparable to ordinary ceramic hydrogen thyratrons.

VII. Conclusions and Recommendations

A working laboratory model of a grid-controlled gaseous switch tube has shown its capability of:

(a) controlling large amounts of microwave pulse energy by using a low potential trigger voltage, i.e., an electronically (voltage-sensitive) controlled device.
(b) short switching times, in the neighborhood of 30 to 40 nanoseconds
(c) broadbanding over the entire C band with a VSWR < 1.2
(d) moderate-to-low loss characteristics when in the active or passive state
(e) good isolation between the incident and transmitted power when in the active state
(f) switching power over a wide range of peak powers from watts to a megawatt
(g) no spike leakage
(h) a recovery time of moderate value

The effects of environmental changes on tube characteristics have not been investigated.

Further work on the switch should tend toward increasing the peak microwave power handling capability and shortening the recovery time. With regard to the former, a program is underway to better understand the r.f. power limitation by constructing an experimental tube with a means of measuring pressure. As regards the latter, a tube is under construction which will be capable of applying pulsed (and delayed) sweeping fields by inserting opposing electrodes in the narrow walls. A study of the methods by which a reduction in arc loss can be accomplished is contemplated.

Another area that should be investigated is that of applying a dc magnetic field parallel to the electric field to cause electron path curvature. This would increase the collision cross section by constricting the electron gas resulting in higher electron densities. This would allow operation at a lower pressure which would increase the rf holdoff fields.

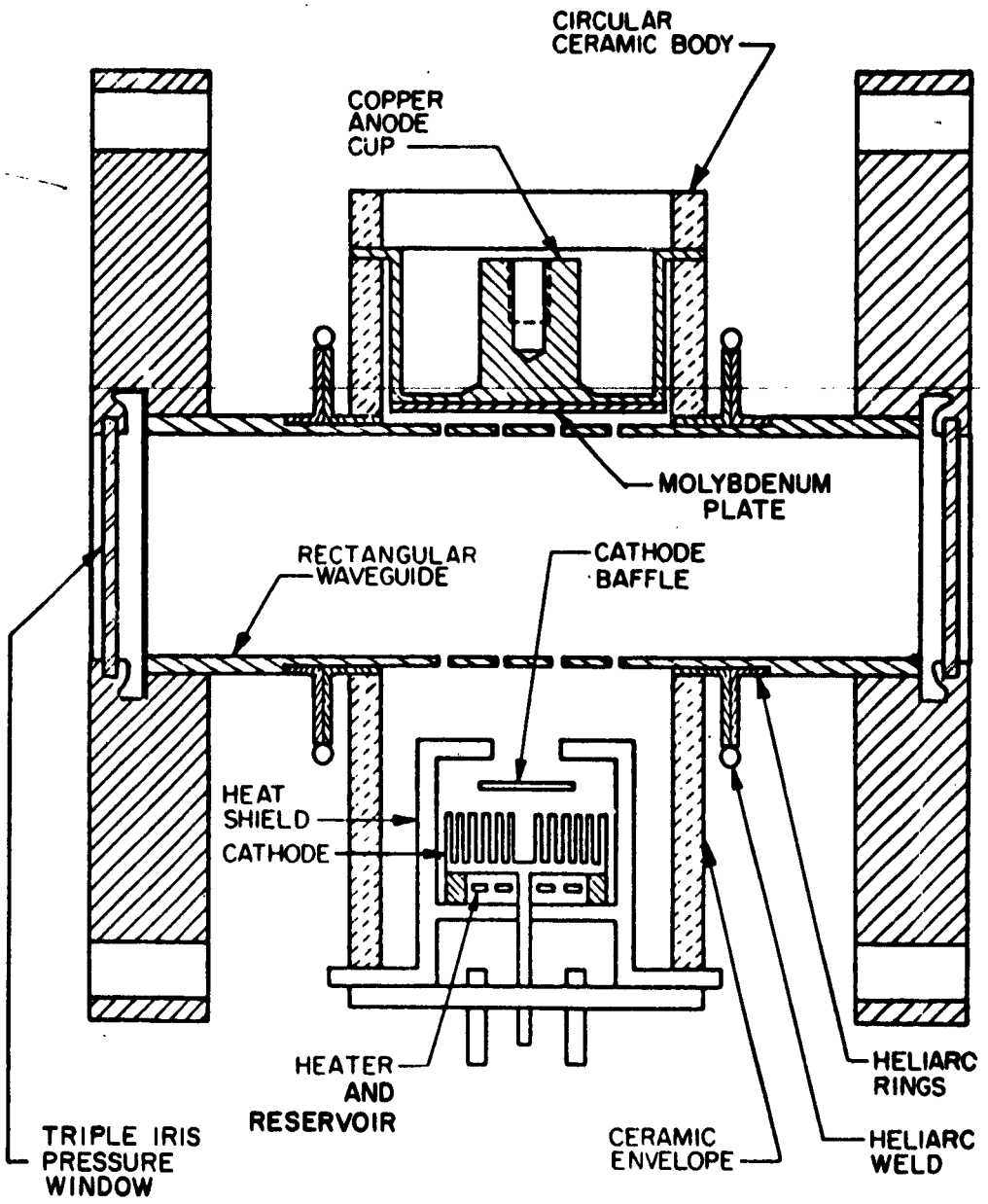

FIG. 1 LOW PRESSURE GAS SWITCH

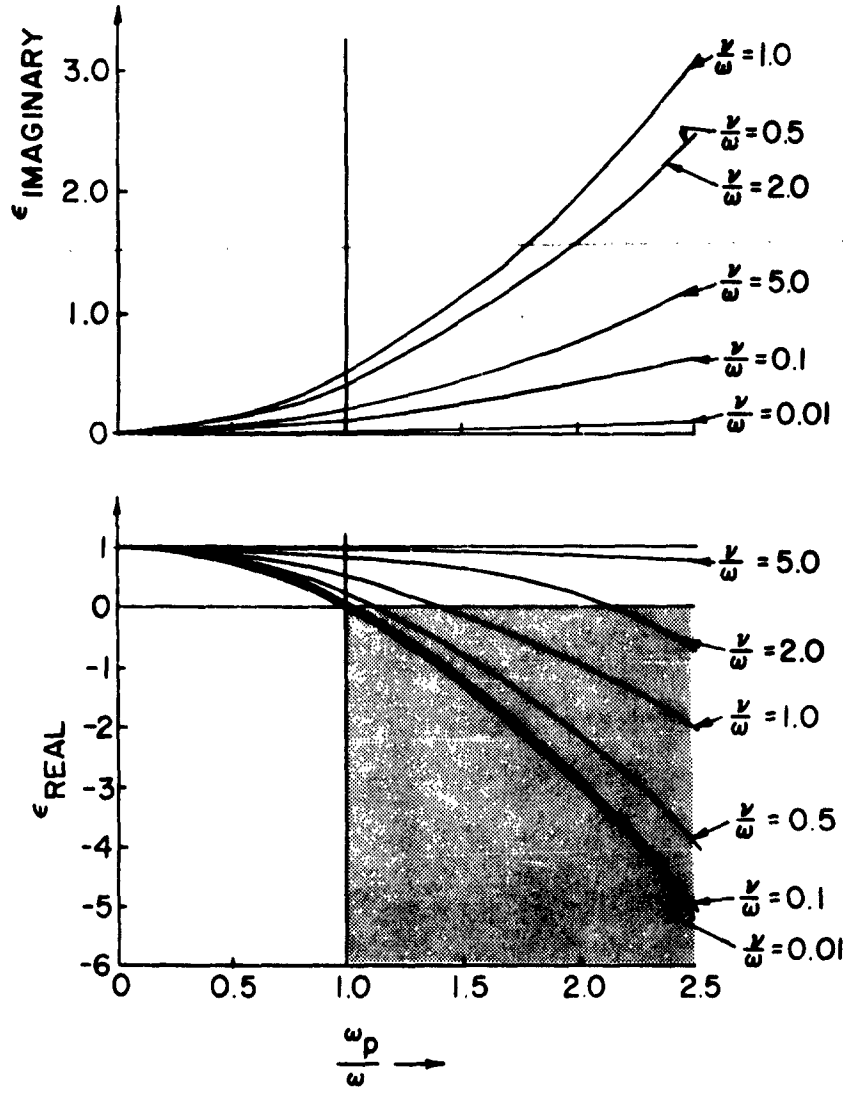

Figs. 2. The Complex Dielectric Constant as a Function of the Plasma Resonance Frequency. ν is The Total Collision Frequency. ω is The Microwave Signal Frequency.

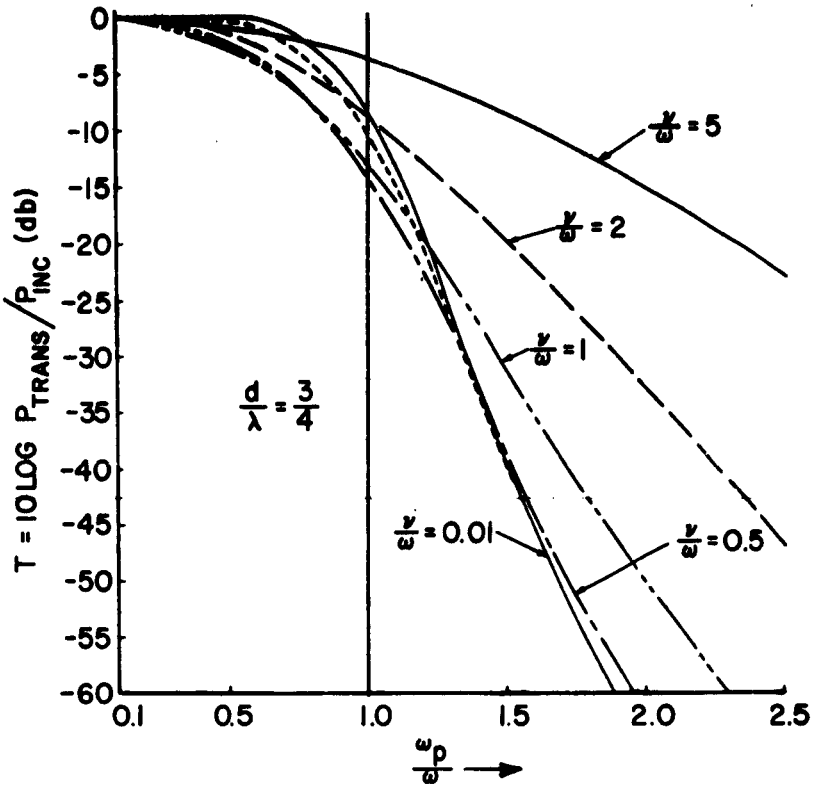

Fig. 3 Transmission in a Plasma of Uniform Density as a Function of Electron Density with Total Collision Frequency as a Parameter

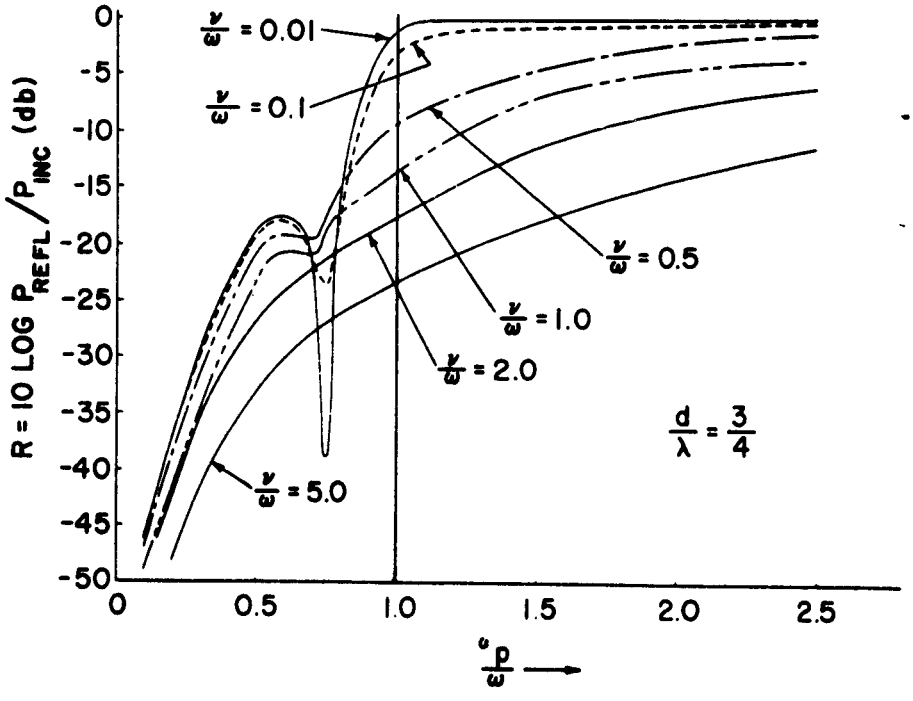

Fig. 4 Reflection in a Plasma of Uniform Density as a Function of Electron Density with Total Collision Frequency as a Parameter

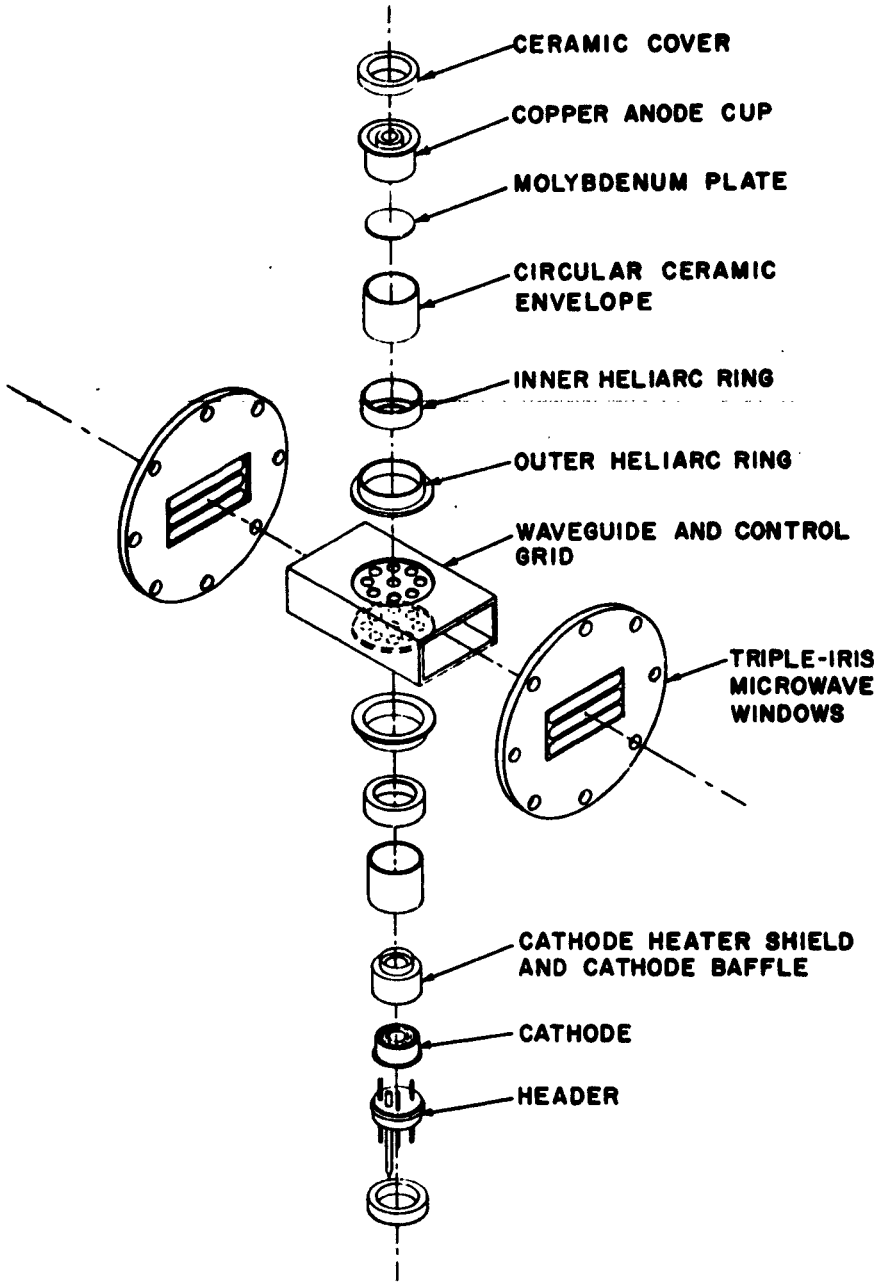

FIG. 5 EXPLODED VIEW - MICROWAVE LOW PRESSURE GAS DISCHARGE SWITCH TUBE

GC-40

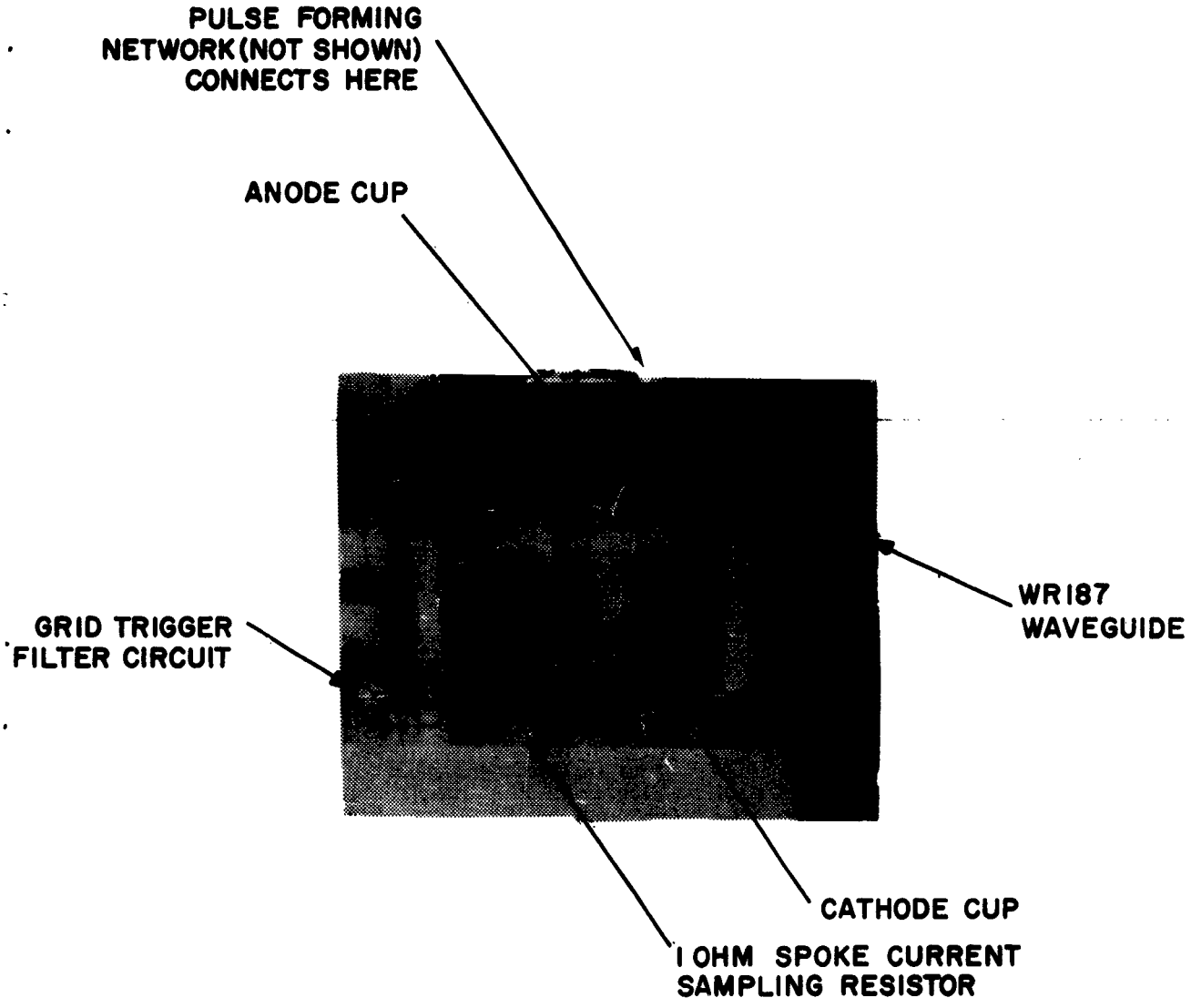

FIG. 6 PHOTOGRAPH OF SWITCH. THE WAVEGUIDE BODY PERFORMS THE DUAL ROLE OF CONTROL GRID FOR GAS TUBE OPERATION AND GUIDING STRUCTURE FOR THE MICROWAVE ENERGY.

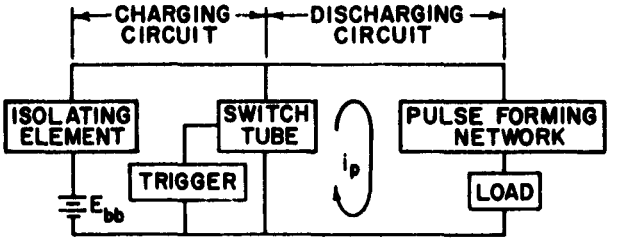

BLOCK DIAGRAM OF CHARGING AND DISCHARGING CIRCUITS

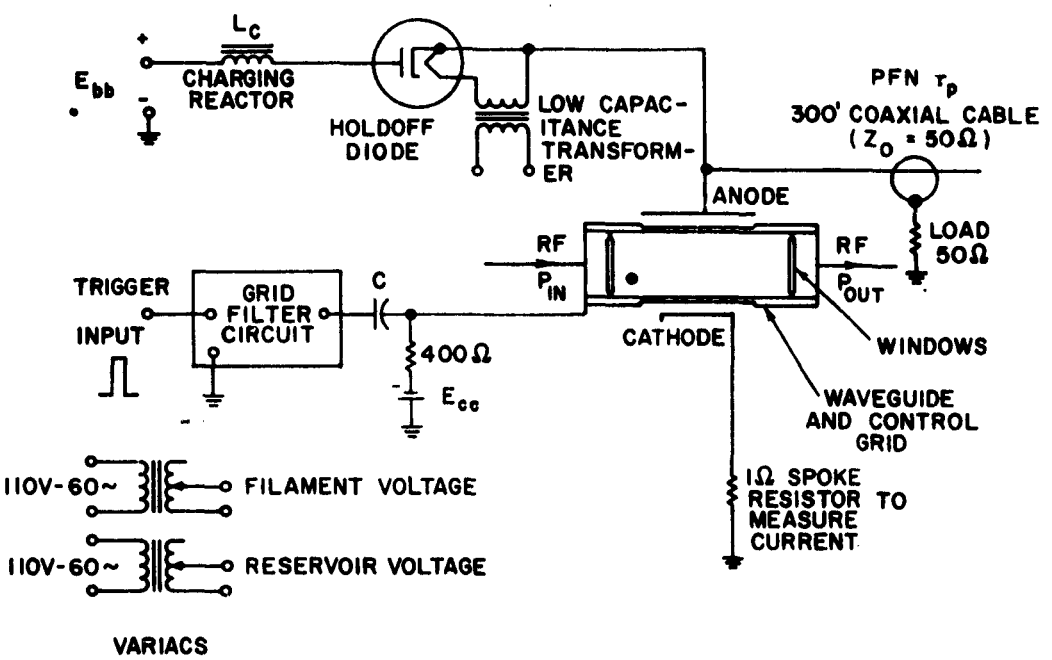

FIG. 7 SCHEMATIC OF MODULATOR

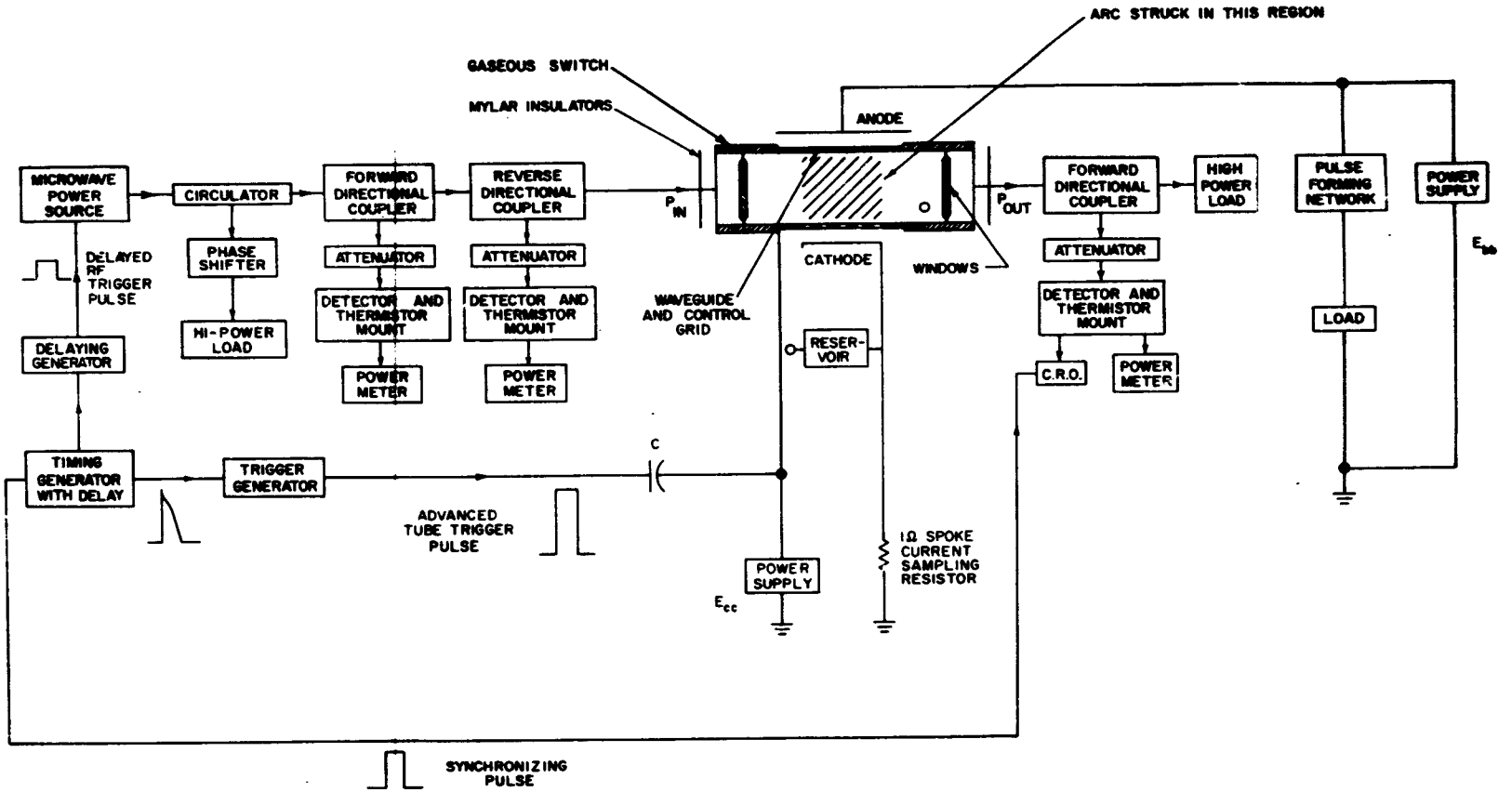

FIG. 8 HIGH POWER TEST FACILITY

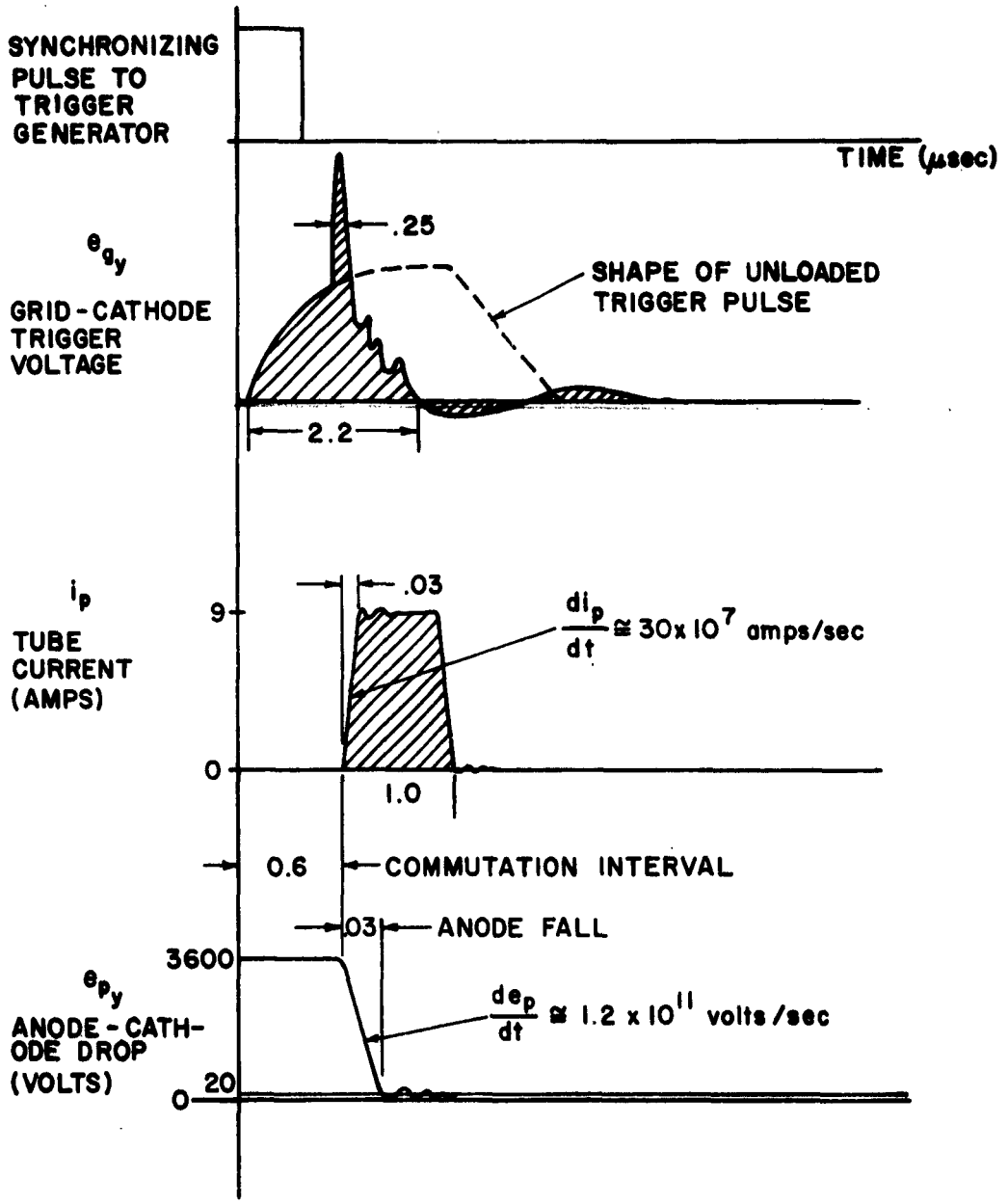

FIG. 9 TYPICAL THYRATRON SWITCH TUBE WAVEFORMS

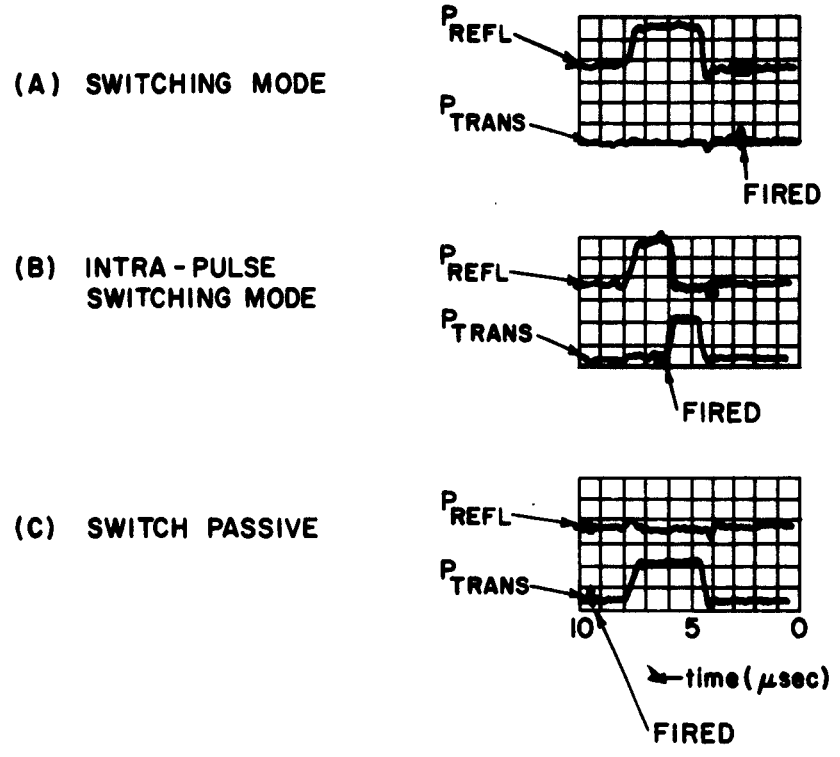

Fig. 10 The P.R.R. is 100 and Pulse Width is 3 Microseconds. RF Power Level is 330 Kilowatts (5.4 RMS KV/CM).

(A) Switch is Fired 1.5 Microseconds Before RF Wave is Incident Resulting in Complete Reflection. Note There is No Spike Leakage.

(B) Switch is Fired 1.5 Microseconds After RF Wave is Incident Resulting in Intra-Pulse Switching Mode. Switch Actuating Time is 30 Nanoseconds.

(C) Switch is Fired 1.5 Microseconds After Passage of the RF Wave Resulting in No Reflection. This Mode Exhibits the RF Holdoff Capability of the Switch.

Figure. 11 **Table I**

TYPICAL SWITCHING DATA OF SWITCH TUBE

	Switching Mode	PRR PPS	T_{rf} μ^s	P_{inc} (Peak	P_{refl} Power in	P_o Kilowatts)	Isolation DB	Arc-Loss DB	Ins. Loss DB
1	Off	200	3	16.6	0.066	16.0			0.15
2	On			16.6	12.6	.0033	35.0	1.2	
3	Off			33.3	0.053	32.6			0.10
4	On			33.3	27.0	0.066	27.0	0.9	
5.	Off			66.6	0.091	66.0			0.05
6	On			66.6	55.0	0.076	29.0	0.8	
7	Off			100.0	0.123	99.8			0.05
8	On			100.0	83.25	0.093	30.0	0.8	
9	Off			133	0.160	132.5			0.05
10	On			133	109.8	0.10	31.0	0.8	
11	Off			226	0.233	220			0.10
12	On			226	186.5	0.10	34.0	0.8	
13	Off			333	4.16	332			0.05
14	On			333	280	0.05	38.0	0.7	
15	Off	100	0.7	681	3.14	645			0.25
16	On			652	565	0.29	35.0	0.6	
17	Off			783(2)	4.73	745			0.21
18	On			755	660	1.60	27.0	0.6	
19	Off			1160	3.60	1110			0.20
20	On			1120	940	0.29	34.0	0.8	
21	Off			1190	5.50	1110			0.30
22	On			1180	940	0.29	36.0	1.0	
23	Off			1380	5.95	1260			0.30
24	On			1450(1)	895	58.4	14.0	2.1	
25	Off	50		1620	9.75	1510			0.30
26	On	50		1680(1)	1130	36.8	17.0	1.7	
27	Off	50		1800	11	1750			0.10
28	On	50		1950(1)	1380	73	14.0	1.5	
29	Off	50	5.0	332	.045	308			0.30
30	On	50	5.0	332	267	0.324	30.0	0.9	

1. **Arcing inside the waveguide could be heard.**
2. **Dynamic measurement of T_s** (clipping time of rf pulse transmitted past tube) was made at this power level.

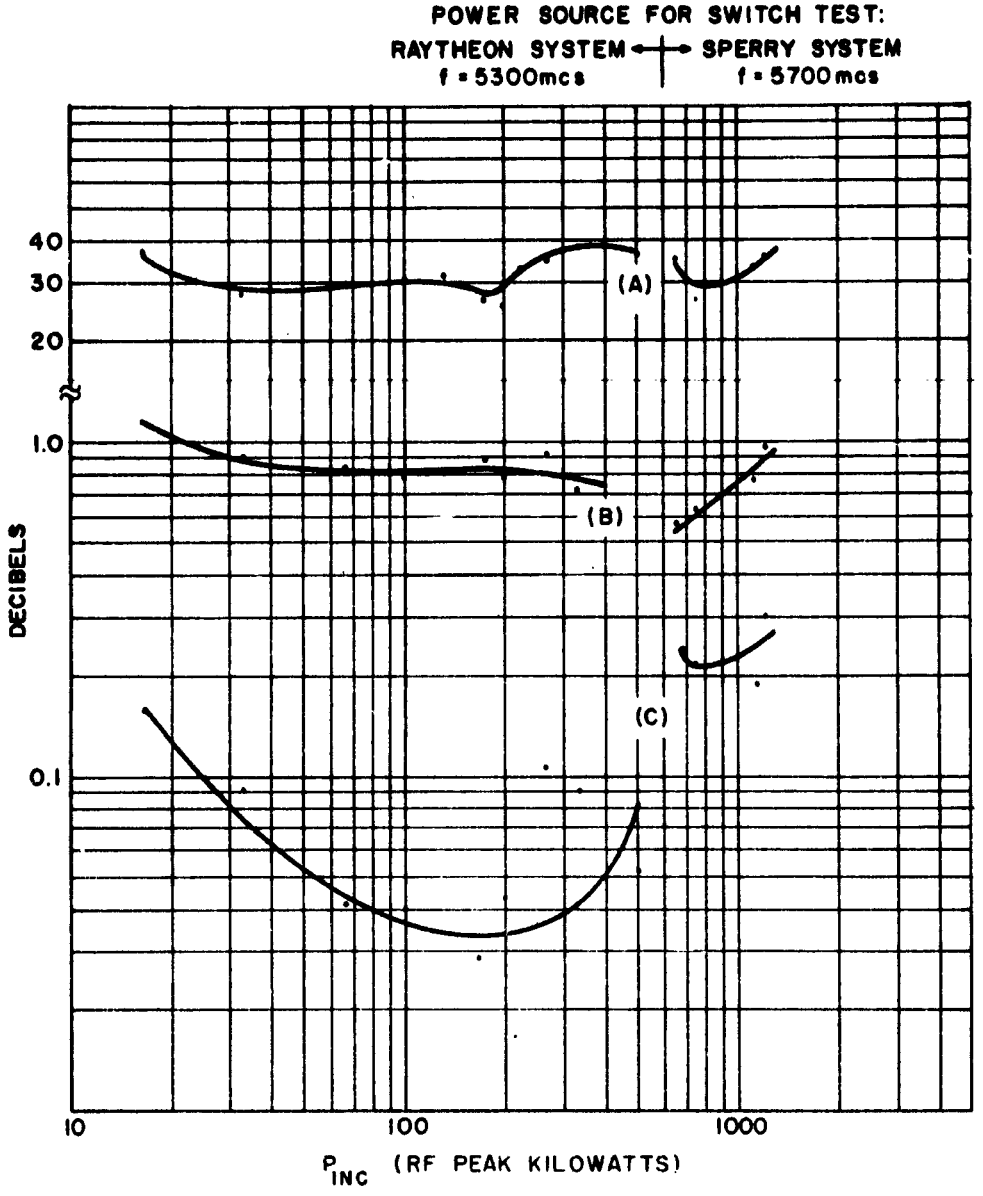

FIG. 12 (A) ISOLATION, (B) ARC LOSS, (C) COLD INSERTION LOSS AS A FUNCTION OF INCIDENT RF POWER

GC-41

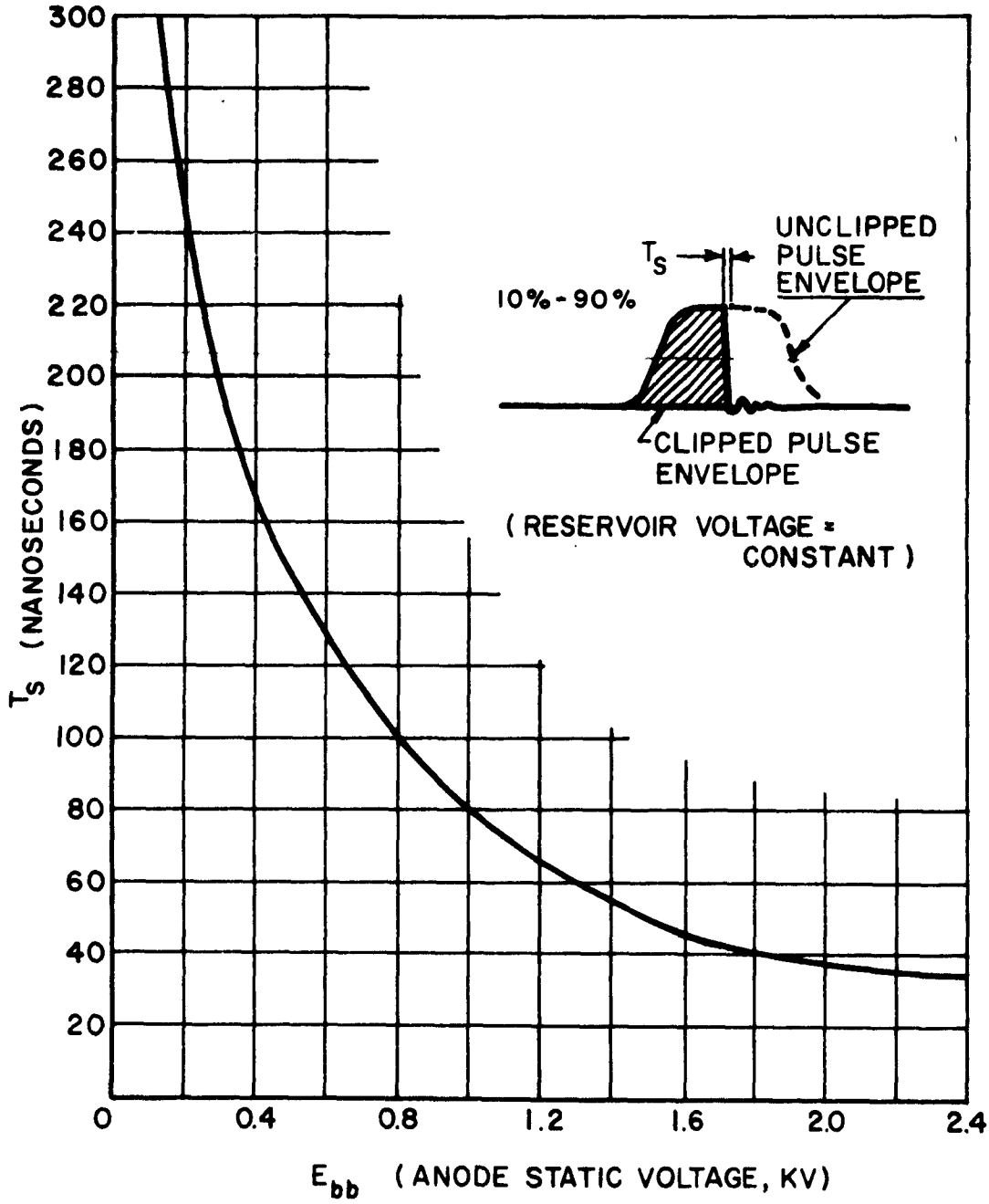

FIG. 13 THE EXPERIMENTAL DEPENDENCE OF THE DYNAMIC SWITCHING TIME AS A FUNCTION OF ANODE VOLTAGE

Figure 14 - Table II

DATA ILLUSTRATING DEPENDENCE OF RF BREAKDOWN FIELD

AS A FUNCTION OF GRID BIAS AND ANODE VOLTAGE

RF Level Necessary to breakdown the gas		Reservoir Voltage	Anode Voltage	Grid Bias	Filament Voltage
P_{inc}	E^*_{inc}(RMS)	E_r	E_{bb}	E_{cc}	E_f
(peak kilowatts)	(kv/cm)	(volts)	(kilovolts)	(volts)	(volts)
270	4.9	3.4	0	0	0
284	5.1	(Pressure is	1.0	0	↓
300	5.2	~0.2 mm of H_g)	2.0	0	↓
310	5.3	↓	3.0	0	↓
334	5.4	↓	3.5	0	↓
302	5.2	↓	1.0	-100	↓
310	5.3	↓	2.0	-100	↓
320	5.35	↓	3.0	-100	↓
334	5.40	↓	3.5	-100	↓
62	2.35	3.4	0	0	6.3
106	3.1	↓	↓	-50	↓
104	3.05	↓	↓	-100	↓
100	3.0	↓	↓	-200	↓
102	3.0	↓	↓	-300	↓
328	5.4	3.0	2.0	0	↓
510	6.7	3.0	2.0	-50	↓
540	7.0	3.0	2.0	-100	↓
560	7.1	3.0	2.0	-200	↓

*at the midplane of the waveguide where the rf field has its maximum value

RECOVERY TIME DATA

Recovery Time* (microseconds)	Anode Voltage (dc kilovolts)	Reservoir Voltage (ac volts)	Grid Bias (volts)
30	1	3.5	-20
36	2	3.5	-20
42	3	3.5	-20
26	1.5	2.5	-20
34	1.5	3.5	-20
36	1.5	4.5	-20
34	1.5	3.5	-10
34	1.5	3.5	-20
34	1.5	3.5	-40
60	1.5	3.5	-80

Fig. 15 Table III

*For definition see Section II.

APPENDIX I

Derivation of the Transmission and Reflection Characteristics of the Microwave Switch

T	=	Normalized Transmitted Power in DB
R	=	Normalized Reflected Power in DB
P_t	=	Normalized Transmitted Power
P_r	=	Normalized Reflected Power
$\bar{v}$	=	Mean Electron Drift Velocity
ω	=	Microwave Signal Frequency
ω_p	=	Plasma Resonance Frequency
ν_c	=	Total Collision Frequency = $\bar{v}\, P_c\, p_o$
b	=	Dummy Variable = $\sqrt{\epsilon}$
ϵ_c	=	Complex Dielectric Constant
ϵ_o	=	Dielectric Constant of Free Space
ϵ	=	Dielectric Constant Relative to ϵ_o
e	=	Electronic Charge
m	=	Electron Mass
λ	=	Free Space Wavelength
β	=	The Complex Propagation Constant
d	=	Distance Along the Z Direction of Transmission
N	=	Electron Density within The Plasma
σ	=	Complex Conductivity of Gaseous Plasma
J	=	Current Density
c	=	Velocity of Light in Vacuo
P_c	=	Probability of Collision $(cm)^{-1}$
p_o	=	Pressure (in mm of Hg)

A qualitative view of the transmission characteristics of the switch tube can be formulated if one employs the impedance concept of transmission line theory. This view is justifiable because guided wave propagation through the switching device does not differ greatly from plane wave propagation through the same unbounded plasma, except for effects of waveguide geometry on the propagating mode or modes. Basic wave properties, thereby, are essentially the same in both cases.

The polarizability and conductivity (excluding the permeability) completely describe the plasma with regard to wave control in the plasma.

The polarizability is the parameter which is most easily controlled in the switch tube. This arises because the sign of the dielectric constant is controlled by the value of N. Variation of the sign of the dielectric constant and, therefore, wave propagation conditions are controlled by the ratio of the plasma resonance frequency ω_p (see equation 3-14) to the electromagnetic field frequency ω. The small loss component of plasma conductivity will be considered in formulating the transmission characteristics. This loss component depends on ν_c/ω. The parameter ν_c is the total collision frequency of the electron with both positive ions and neutral gas molecules. These collisions cause an in-phase oscillatory component of electron motion with regard to the incident microwave field thereby causing some power absorbtion by the gas. Ratios of ν_c/ω from 0.01 to 10 will be used.

Reference to the adjoining figure shows the idealized regions of the bounded plasma. The plasma is assumed to contain an isotropic dielectric of uniform density.

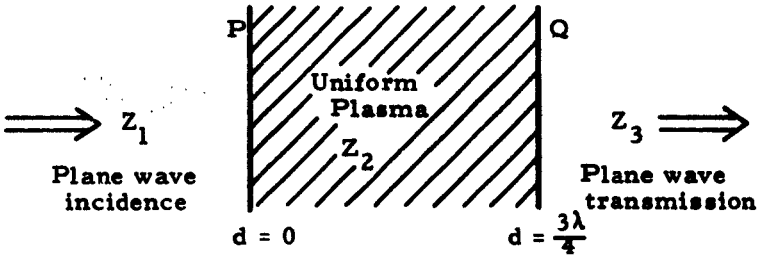

IDEALIZED REGIONS OF SWITCH TUBE

The problem is one of determining the reflected and transmitted powers due to multiple reflections at plasma surfaces P and Q.

There are five quantities of interest:

(AI-1) The incident wave $E_i = E_o \epsilon^{j\beta_1 z}$; $H_i = \frac{1}{Z_1} E_i$

(AI-2) The reflected wave $E_r = E_1 \epsilon^{-j\beta_1 z}$; $H_r = -\frac{1}{Z_1} E_2$

(AI-3) The field within the plasma

$$E_m = E_2^+ \epsilon^{j\beta_2 z} + E_2^- \epsilon^{-j\beta_2 z}$$

$$H_m = \frac{1}{Z_2}\left(E_2^+ \epsilon^{j\beta_2 z} - E_2^- \epsilon^{-j\beta_2 z}\right)$$

(AI-4) The transmitted portion $E_t = E_3 \epsilon^{j\beta_3 z}$; $H_t = \frac{1}{Z_3} E_t$

The boundary conditions are defined

at P $$E_o + E_1 = E_2^+ + E_2^-$$

at P $$E_o - E_1 = \frac{Z_1}{Z_2}\left(E_2^+ - E_2^-\right)$$

at Q $$E_2^+ \epsilon^{j\beta_2 d} + E_2^- \epsilon^{j\beta_2 d} = E_3 \epsilon^{j\beta_3 d}$$

at Q $$E_2^+ \epsilon^{j\beta_2 d} + E_2^- \epsilon^{-j\beta_2 d} = \frac{Z_2}{Z_3} E_3 \epsilon^{j\beta_3 d}$$

Solving for E_1/E_o and E_3/E_o

(A1-5) $$\frac{E_1}{E_o} = \frac{E_r \varepsilon^{+j\beta_1 z}}{E_i \varepsilon^{j\beta_1 z}} = \frac{\left(1 - \frac{Z_1}{Z_2}\right)\left(1 + \frac{Z_2}{Z_3}\right) + \left(1 + \frac{Z_1}{Z_2}\right)\left(1 - \frac{Z_2}{Z_3}\right)\varepsilon^{2j\beta_2 d}}{\left(1 + \frac{Z_1}{Z_2}\right)\left(1 + \frac{Z_2}{Z_3}\right) + \left(1 - \frac{Z_1}{Z_2}\right)\left(1 - \frac{Z_2}{Z_3}\right)\varepsilon^{2j\beta_2 d}}$$

(A1-6) $$\frac{E_3}{E_o} = \frac{E_t \varepsilon^{-j\beta_3 z}}{E_i \varepsilon^{-j\beta_1 z}} = \frac{4\varepsilon^{j\beta_2 d}}{\left(1 + \frac{Z_1}{Z_2}\right)\left(1 + \frac{Z_2}{Z_3}\right) + \left(1 - \frac{Z_1}{Z_2}\right)\left(1 - \frac{Z_2}{Z_3}\right)\varepsilon^{2j\beta_2 d}}$$

The intrinsic impedance $Z_1 = Z_3 = Z_o$ and $Z_2 = Z_o \frac{1}{\sqrt{\varepsilon}} = Z_o \frac{1}{b}$;

hence $b = \sqrt{\varepsilon}$ $\beta_1 = \beta_3$ and $\beta_2 = \frac{\omega}{c} b = \frac{2\pi b}{\lambda}$.

Inserting these parameters into (5) and (6) and squaring the absolute values yields the (normalized) reflected and transmitted powers.

(A1-7) $$P_r = \frac{\text{Power Reflected}}{\text{Power Incident}} = \left| \frac{(1 - b^2)\ (1 - \exp(4\pi\, jbd/\lambda))}{(1+b)^2 - (1-b)^2 \exp(4\pi\, jbd/\lambda)} \right|^2$$

(A1-8) $$P_t = \frac{\text{Power Transmitted}}{\text{Power Incident}} = \left| \frac{4b \exp(2\pi\, jbd/\lambda)}{(1+b)^2 - (1-b)^2 \exp(4\pi\, jbd/\lambda)} \right|^2$$

The switch tube is 3/4 of a wavelength long. Substitution of this value yields the expression used in the report. The entire transmission properties, therefore, depend on one parameter, b, which is a function of the gas characteristics, the incident microwave frequency, and the tube geometry.

The equivalent dielectric constant of the plasma, described by b, can be found by using the equation of motion for electrons given below. (This assumes that electron current predominates and that ion current is negligible.)

(A1-9) $$m \frac{d\, v(t)}{dt} + m\, \nu_c\, v(t) = -\, e\, E_o\, \varepsilon^{-j\omega t}$$

The drift velocity of the n (electrons/cc) free electrons is

(A1-10) $$v(t) = \frac{-\, e\, E_o\, \varepsilon^{-j\omega t}}{(\nu_c - j\omega)\, m} = v_o\, \varepsilon^{-j\omega t}$$

The current, made up of the real and displacement currents is

(A1-11) $$J = -\, Ne\, v(o) = \frac{Ne^2\, E_o}{m(\nu_c - j\omega)} = \frac{Ne^2}{m} \left(\frac{\nu_c}{\nu_c^2 + \omega^2} - j \frac{\omega}{\nu_c^2 + \omega^2} \right) E_o$$

(A1-12) $$\nabla \times \underline{H} = \underline{J} + \frac{\partial \underline{D}}{\partial t} ,$$

(A1-13) $$\nabla \times \underline{H} = \underline{J} - j\omega\varepsilon_o\, \underline{E} = \frac{Ne^2\, \underline{E}}{m(\nu_c - j\omega)} - j\omega\varepsilon_o\, \underline{E}$$

The equivalent dielectric constant is shown between the square brackets

(A1-14) $$\nabla \times \underline{H} = j\omega\varepsilon_o \left[1 - \frac{Ne^2}{m\, \varepsilon_o \left(\omega^2 + \nu_c^2\right)} + j \left(\frac{\nu_c}{\omega}\right) \frac{Ne^2}{m\, \varepsilon_o \left(\omega^2 + \nu_c^2\right)} \right] \underline{E}$$

The dummy variable b is defined as $\sqrt{\varepsilon_i/\varepsilon_o} = \sqrt{\varepsilon}$. Hence

A1-15) $$b = \left[1 - \frac{\omega_p^2}{\omega^2 + \nu_c^2} + j \left(\frac{\nu_c}{\omega}\right) \frac{\omega_p^2}{\omega^2 + \nu_c^2} \right]^{1/2} \quad ; \quad \omega_p^2 = \frac{Ne^2}{m\, \varepsilon_o}$$

It is assumed that the mean total collision frequency ν_c is independent of the drift velocity. This restriction is not prohibitive because certain gases exhibit a slowly varying ν_c with changing potentials. S.C. Brown has shown that helium exhibits a mean collision frequency depending only on pressure.

APPENDIX II

Derivation of the Breakdown Field for Pulsed Discharges

The continuity equation for electrons is:

$$\frac{\partial N}{\partial t} = P_e - L_e = \nu_c N - \nabla^2 DN \tag{A2-1}$$

where $\nu_i N$ is the number of new electrons produced per second and $\nabla^2 DN$ is the number of electrons lost by diffusion per second. To a first approximation $\nabla^2 DN$ may be replaced by $- N/\Lambda^2$, then integrating over time (the duration of the applied field) yields

$$\int_{N_o}^{N_B} \frac{dN}{N} = \int_o^{\tau} (\nu_i - \frac{D}{\Lambda^2})\, dt \tag{A2-2}$$

where breakdown occurs at time τ for an electron concentration of N_B. The solution, after dividing both sides by the pressure, is:

$$\frac{1}{p\tau} \ln \frac{N_B}{N_o} = \frac{\alpha}{p} \bar{v}_d - \frac{Dp}{(p\Lambda)^2} \qquad \text{where } \frac{\alpha}{p} = f\left(\frac{E_e}{p}\right) \tag{A2-3}$$

where $\alpha \bar{v}_d$ has been substituted for ν_i. The coefficients as a function of the effective electric fields are then determined to yield the threshold field values. This has been done by Gould and Roberts[6] in the high pressure ranges and by MacDonald[9] in the low pressure range. Both papers deal with air however.

BIBLIOGRAPHY

1. Hill, R.M. and Ichiki, S.K., "Rapid Microwave Switching with Low Pressure Arcs", Final Reports, Rome Air Development Center, Rome, New York (July, 1959).
2. Bradley, E.M., Pringle, D.H., Journal of Electronics VI, p. 389 (January, 1956).
3. Goldstein, L., and Cohn, N.L., Phys. Rev. 73, p. 83 (January, 1948).
4. "Fourth Quarterly Letter Report", PIBMRI 853.4-61, Polytechnic Institute of Brooklyn, (May 9, 1961).
5. Goldstein, L., Chapter on Gaseous Electronics in "Advances in Electronics and Physics", Vol. VII, Academic Press, (1955).
6. Gould L., and Roberts, L.W., Jour. Appl. Phy. No. 27, p. 1162, (October, 1956).
7. S.C. Brown, Basic Data of Plasma Physics, Wiley, (1959).
8. Goldstein, L., "Final Report on T-R Tube Spike Leakage Investigation", E.E. Research Laboratory, Univ. of Illinois, Urbana, Ill., (October, 1955).
9. MacDonald, A.D., "High-Frequency Breakdown in Air at High Altitudes", Proc. I.R.E., Vol. 47, pp. 436-441, (March, 1959).
10. Strum, P.D., "A Note on Noise Temperatures", Trans. IRE., Vol. MTT-4, pp. 145-151; July 1956.

DISTRIBUTION LIST FOR CONTRACT REPORTS

	No. of Copies
**RADC (RALTM, ATTN: Mr. Vannicola) Griffiss AFB, NY	3
*RADC (RAAPT) Griffiss AFB, NY	1
*RADC (RAALD) Griffiss AFB, NY	1
GEEIA (ROZMCAT) Griffiss AFB, NY	1
*RADC (RAIS, ATTN: Mr. Malloy) Griffiss AFB,	1
*US Army Electronics R & D Labs. Liaison Officer RADC Griffiss AFB, NY	1
*AUL (3T) Maxwell AFB, Ala.	1
ASD (ASAPRD) Wright-Patterson AFB, Ohio	1
Chief, Naval Research Lab. ATTN: Code 2027 Washington 25, DC	1
Air Force Field Representative Naval Research Lab ATTN: Code 1010 Washington 25, DC	1
Commanding Officer US Army Electronics R & D Labs. ATTN: SELRA/SL-ADT Ft. Monmouth, NJ	1
AFSC (SCSE) Andrews AFB Washington 25, DC	1
Commanding General US Army Electronics Proving Ground ATTN: Technical Documents Library Ft. Huachuca, Ariz.	1
*ASTIA (TISIA-2) Arlington Hall Station Arlington 12, Va.	10

	No. of Copies
Commanding Officer US Army Electronics R & D Labs. ATTN: SELRA/SL-PEE/Mr. Lipetz Fort Monmouth, N.J.	1
Bureau of Ships - 691B2C Electronics Division ATTN: Mr. Leo V. Gumina Room 3329 Main Navy Bldg. Washington 25, DC	1
Airborne Instruments Laboratory ATTN: Mr. Avery ~~Deer Park, L.I., N.Y.~~	1
General Electric Co. Heavy Military Electronics Dept. ATTN: Dr. Joseph C. Almasi Syracuse, N.Y.	1
ESD ATTN: S. Herskovitz LG Hanscom Field Bedford, Mass.	1
Scientific Engineering Institute ATTN: Mr. Daniel Schwarzkoph 140 Fourth Ave. Waltham, Mass.	1
Cornell Aeronautical Laboratory ATTN: Mr. Beitz Buffalo, N.Y.	1
General Engineering Lab. ATTN: George E. Feiker Schenectady, N.Y.	1
AFPR General Electric Co. Lockland Br PO Box 91 Cincinnati 15, Ohio	1
Chief, Bureau of Ships Dept. of the Navy Main Navy Bldg. Washington 25, DC Code 312	1
Dielectric Products Company ATTN: Dr. Charles Brown Raymond, Maine	1

	Nr. of Copies
Airborne Instruments Lab ATTN: Mr. Avery Deer Park, LI, NY	1
General Electric Co. Heavy Military Electronics Dept ATTN: Dr. Joseph C. Almasi Syracuse, NY	1
ESD ATTN: S. Herskovitz LG Hanscom Field Bedford, Mass.	1
Scientific Engineering Institute ATTN: Mr. Daniel Schwarzkoph 140 Fourth Ave. Waltham, Mass.	1
Cornell Aeronautical Lab ATTN: Mr. Beitz Buffalo, NY	1
General Engineering Lab ATTN: George E. Feiker Schenectady, NY	1